

Learning Object-Centric Spatial Reasoning for Sequential Manipulation in Cluttered Environments

Chrisantus Eze^{1*}, Ryan C Julian² and Christopher Crick¹
Oklahoma State University¹, Google DeepMind²

Abstract—Robotic manipulation in cluttered environments presents a critical challenge for automation. Recent large-scale, end-to-end models demonstrate impressive capabilities but often lack the data efficiency and modularity required for retrieving objects in dense clutter. In this work, we argue for a paradigm of specialized, decoupled systems and present Unveiler, a framework that explicitly separates high-level spatial reasoning from low-level action execution. Unveiler’s core is a lightweight, transformer-based Spatial Relationship Encoder (SRE) that sequentially identifies the most critical obstacle for removal. This discrete decision is then passed to a rotation-invariant Action Decoder for execution. We demonstrate that this decoupled architecture is not only more computationally efficient in terms of parameter count and inference time, but also significantly outperforms both classic end-to-end policies and modern, large-model-based baselines in retrieving targets from dense clutter. The SRE is trained in two stages: imitation learning from heuristic demonstrations provides sample-efficient initialization, after which PPO fine-tuning enables the policy to discover removal strategies that surpass the heuristic in dense clutter. Our results, achieving up to 97.6% success in partially occluded and 90.0% in fully occluded scenarios in simulation, make a case for the power of specialized, object-centric reasoning in complex manipulation tasks. Additionally, we demonstrate that the SRE’s spatial reasoning transfers zero-shot to real scenes, and validate the full system on a physical robot requiring only geometric workspace calibration; no learned components are retrained.

I. INTRODUCTION

Retrieving an occluded object from dense clutter requires solving two distinct sub-problems: which objects to remove and in what order, then how physically to remove each one. Methods that conflate these, mapping pixels directly to grasp actions [1]–[4], force a single model to solve object selection and execution jointly, which scales poorly as scene complexity grows. Large-scale end-to-end and vision-language-action (VLA) approaches [5]–[7] offer impressive generality, but at either a prohibitive cost or with long inference latencies exceeding 6,000ms per decision (see Table I), neither of which fits the tight budgets of real manipulation systems.

We argue that explicit decomposition is the right inductive bias for this problem. By separating a lightweight spatial reasoning module, which identifies the next obstacle, from a dedicated execution module, which removes it, each component learns a strictly simpler problem, failures become independently diagnosable, and the system remains deployable on resource-constrained hardware. The Unveiler’s Spatial Relationship Encoder (SRE) and Action Decoder utilize only

83.03M parameters yet achieve 97.6% success in partially occluded scenarios, outperforming models with significantly larger parameter counts, such as [8]–[10], by over 20% (see Tables I and II). Furthermore, we show that VLAs can reason spatially in simple scenes but degrade in dense clutter.

Our primary contributions are:

- **A decomposed architecture for cluttered manipulation** that separates spatial reasoning from action execution, enabling the SRE to focus on obstacle dependency modeling, while the Action Decoder handles robust push-grasp execution. This decomposition yields 15–40% higher success rates than monolithic approaches across varying clutter densities.
- **A transformer-based spatial relationship encoder** that learns to identify optimal obstacle removal sequences from heuristic demonstrations, achieving up to 97.6% accuracy in densely cluttered scenes in simulation.
- **A two-stage SRE training pipeline** in which imitation learning from heuristic demonstrations initializes the policy sample-efficiently, and PPO fine-tuning then enables the SRE to discover removal sequences that surpass the heuristic in dense, fully occluded scenes.

We train our framework entirely using simulated demonstrations in PyBullet [11] and evaluate it across multiple scene complexities (ranging from 2 - 12 objects), levels of target occlusion, and both simulated and real-world settings. Our results show that Unveiler significantly outperforms strong baselines in terms of task completion and planning efficiency. By focusing on the specific problem of “unveiling” a target, our work makes a case for the continued relevance of purpose-built systems in an era of large-scale models, which can serve as a complement.

II. RELATED WORK

Our work builds upon and extends existing work in robotic manipulation, particularly in the areas of push-grasping synergy, object-centric representation learning, and foundation models for robotics.

A. Push-Grasping Synergy

The concept of coordinating pushing and grasping actions to manage clutter and improve grasping success is a well-established area of research [1], [12]–[14]. Early work, such as [12], introduced the idea of using self-supervised deep RL to learn the synergistic relationship between pushing and grasping. The TransporterNet architecture [2], a significant

*Corresponding author

²This work was done when Ryan C. Julian was at Google DeepMind

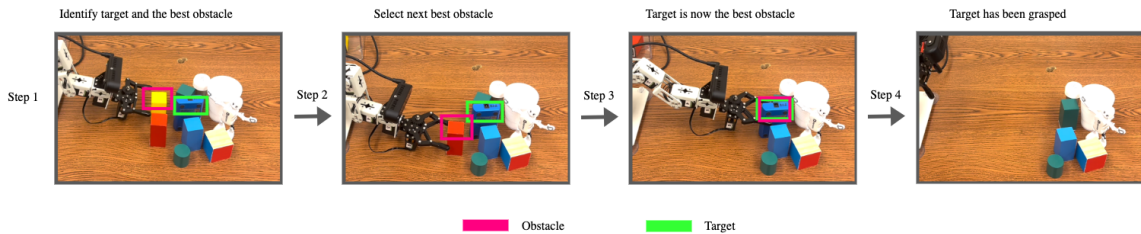


Fig. 1. Unveiling occluded targets through strategic obstacle removal. Given a cluttered scene with objects of similar shapes and colors, our approach identifies which obstacles must be removed and in what order to access the target object (blue object), solving the spatial reasoning challenge before action execution.

advancement, uses a fully convolutional network to learn visuomotor policies for both pushing and grasping, demonstrating impressive performance in cluttered environments. However, TransporterNet and its successors often rely on a two-stage process, first pushing to clear space and then grasping, without a more integrated approach to manipulation.

More recent methods have sought to improve upon this two-stage paradigm [3], [4]. MPGNet [4], for example, introduces a network that learns to synergize “move”, “push”, and “grasp” actions for more efficient target-oriented grasping in occluded scenes. This work, along with others, highlights a trend toward more integrated and dynamic action selection. Our work contributes to this line of research by proposing a novel object-centric representation that allows for more nuanced spatial reasoning and a more flexible approach to sequential manipulation. Unlike methods that primarily focus on clearing clutter, our approach reasons about the spatial relationships between objects to inform a sequence of actions, leading to more efficient and successful manipulation in highly cluttered scenes.

B. Object-centric Representation Learning

A central challenge in robotic manipulation is learning representations that capture object properties and their relations. Early approaches such as VIMA [15] and VIOLA [16] employed imitation learning with language prompts and object proposals, but their effectiveness is constrained by the diversity and quality of demonstrations. More recent work emphasizes object-centric world models to improve generalization and exploration. For instance, [17] constructs 3D object-centric representations that enable manipulation policies robust to viewpoint changes and novel objects, while FOCUS [18] learns an object-centric world model to guide exploration and planning.

Our approach departs from these by tailoring object-centric reasoning specifically to sequential manipulation in dense clutter. Instead of focusing primarily on generalization, we explicitly encode long-horizon spatial dependencies and occlusion relationships, yielding interpretable decision-making. This design not only facilitates trust and validation since the selection probabilities allow inspection of which object the model prioritized and why, but also enhances robustness in multi-step planning, such as clearing obstacles before grasping a target.

C. Vision-Language Models for Robotic Manipulation

The integration of large language models (LLMs) and vision-language models (VLMs) [19] has opened new frontiers in robotics. Models like ThinkGrasp [10], OVGNet [20], and VILG [8] leverage the semantic understanding of VLMs to enable more intuitive and flexible robotic grasping. ThinkGrasp, for example, uses a VLM to reason about grasping in clutter, allowing for more strategic and context-aware manipulation. OVGNet provides a unified framework for open-vocabulary robotic grasping, enabling robots to grasp objects based on natural language descriptions. VILG, meanwhile, proposes a framework for language-conditioned grasping in clutter, employing CLIP [9] for grounding vision and language prompts.

While these models demonstrate the power of VLMs for high-level reasoning, they often come with significant computational overhead and can be less focused on the fine-grained spatial understanding necessary for robust low-level motor control. Our work complements these advancements by proposing a lightweight and specialized architecture. Instead of relying on a monolithic VLM for both high-level planning and low-level control, our model uses a focused, object-centric representation for precise physical interaction. This approach is not only more computationally efficient but also enhances robustness and interpretability at the manipulation level. By bridging the gap between high-level commands and the precise, low-level actions required to execute them, our model offers a more complete and practical solution for sequential manipulation in complex, real-world scenarios.

III. PROBLEM FORMULATION AND DECOMPOSITION

We study sequential target retrieval from dense clutter using a top-down RGB-D perception stack and a push-grasp primitive. Given an RGB scene image I and corresponding depth heightmap I_g (constructed from the fused RGB-D point cloud), instance segmentation produces a set of object masks $M = \{M_1, \dots, M_N\}$ and a target index t . We use heightmaps rather than raw depth images because they provide a robot-centric, top-down representation that reduces perspective distortion and yields a consistent action reference frame.

Segmentation mismatch. In clutter, the number of detected instances may differ from the true object count. We denote by N the number of predicted masks at the current

step; Unveiler predicts and executes one action per step, so each removal typically improves visibility and reduces segmentation errors over time.

Action primitive and constraints. Following Kiatos et al. [3], the robot executes a push-grasp primitive under the constraints: (i) fixed end-effector height during execution, (ii) constant aperture during the push phase, (iii) heightmap boundaries aligned with workspace limits, and (iv) a 0.5 m \times 0.5 m tabletop workspace.

At each decision step, the robot must (a) choose which visible object to remove next and (b) execute a continuous push-grasp action to remove it. Unveiler factorizes this into a discrete object-selection policy (SRE) and a conditional action-execution policy (Action Decoder):

$$\pi(a | s) = \sum_{i \in \{1, \dots, N\}} \pi_{\text{SRE}}(i | s, t) \pi_{\text{AD}}(a | s, i), \quad (1)$$

where the state s comprises the scene observation (including I and/or I_g) and the set of instance masks/crops M with target index t , the discrete choice i indexes an object instance, and $a \in \mathbb{R}^4$ parameterizes the push-grasp primitive (position, orientation, aperture). This decomposition enables the SRE to focus on object-centric spatial reasoning (which obstacle is most critical), while the Action Decoder focuses on robust, rotation-invariant execution for the selected object.

This factorization reduces the learning problem to multiclass object selection and yields an interpretable bound relating end-task performance to SRE selection error (Section V).

IV. PROPOSED APPROACH

While traditional approaches often focus solely on identifying the nearest obstacles to a target object [1], [13], [21]–[24], our method tackles the more complex task of identifying an optimal removal sequence to access a target object, requiring spatial reasoning well beyond simple proximity to the target object. Our framework determines the next object to remove based on two spatial criteria: (i) the distance to the workspace boundary (periphery), which serves as a proxy for grasp accessibility, as peripheral objects tend to be less occluded and more readily reachable by the robot; and (ii) the distance from the target, which prioritizes objects in closest proximity to the obstructed region. Scene stability is promoted implicitly: by removing peripheral objects first, the method minimizes disturbance to objects located deeper within the pile, thereby reducing the likelihood of cascade effects.

To tackle these challenges effectively, we decompose our approach into two complementary components: a Spatial Relationship Encoder (Section IV-A) that identifies the critical objects to be removed, and an Action Decoder (Section IV-B) that executes the physical manipulation required to clear the path and retrieve the target. This decomposition allows us to separately optimize the perception and manipulation aspects of the task while maintaining their natural interdependence.

A. Spatial Relationship Encoder

While the heuristic (Algorithm 1) provides effective demonstrations in moderate clutter, it operates on geometric primitives (centroid positions and boundary distances) that become unreliable under dense occlusion and imperfect segmentation. The SRE is designed to internalize the same spatial logic into learned visual representations, gaining robustness to segmentation noise and the ability to capture higher-order object dependencies that the heuristic’s additive scoring cannot model.

The key challenge in object manipulation in cluttered environments is identifying which obstacles to remove to access a target object. We formulate this as a spatial dependency modeling problem that learns to understand and leverage relationships between the target and surrounding objects. Our approach uses purely learned representations to predict the optimal sequence of objects to remove.

The SRE is a transformer encoder model [25] and takes as input the top-camera view image of the scene, a cropped view of the target object, and the cropped views of all visible objects in the scene. The architecture is designed to output a discrete decision: the index of the object that should be removed next. These indices correspond directly to the N object bounding boxes detected by the segmentation model, where each detected object is assigned a sequential index from 0 to $N-1$. The SRE then outputs a probability distribution over these N indices, selecting the object with the highest removal probability. Invalid indices (those exceeding the current object count) are automatically filtered out during inference.

The inputs are normalized and replicated across three channels to match the expected input format. Visual features are then extracted using a ResNet18 [26] backbone pretrained on ImageNet [27], transforming each $1 \times 144 \times 144$ image into a 1×1024 feature map for both the target and the N object crops. These features are flattened and passed through multi-layer perceptrons (MLPs) to obtain 1024-dimensional latent representations. A multi-head attention mechanism computes attention scores between the target (as query), scene image (as key), and the surrounding objects (as value). An MLP further processes the resulting $N \times 512$ attention output to produce $1 \times N$ removal weights for each object.

To model inter-object dependencies and target relevance, we employ a stack of transformer blocks. These layers enable the model to capture higher-order relationships such as indirect occlusions (i.e., an object indirectly blocking the target by being in front of another obstacle).

The output of this module is a selection mask highlighting which object should be passed to the Action Decoder for manipulation. This discrete selection mechanism enables sequential decision making, where only one object is removed per step, allowing the robot to reduce occlusion and scene clutter iteratively.

SRE Training: The SRE is trained in two stages. In the first stage, the policy is initialized via imitation learning (IL) on demonstrations generated by the scoring heuristic in Algorithm 1. This encodes the geometric removal logic

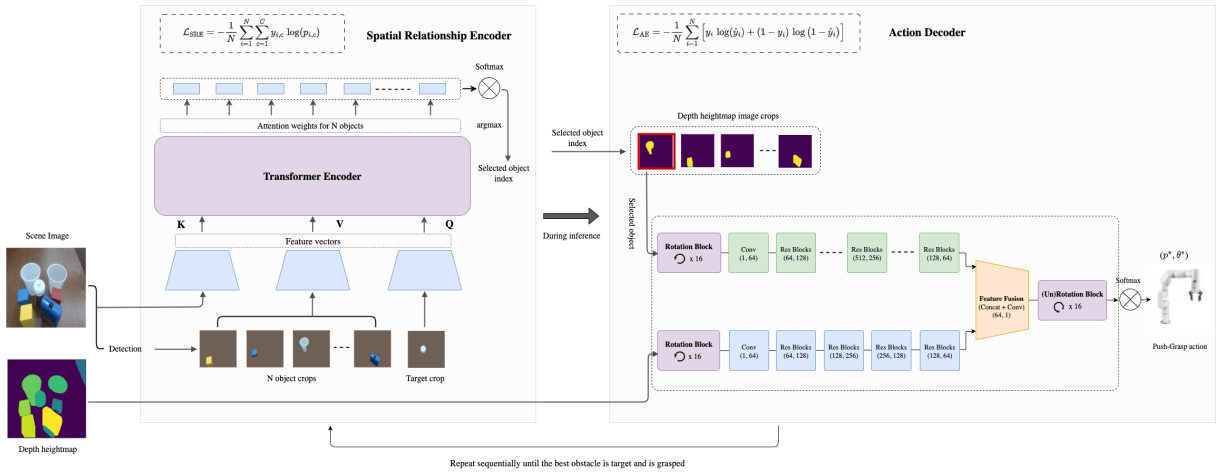


Fig. 2. Unveiler system architecture. Independent training of the SRE and Action Decoder enables each component to specialize in its respective task while sharing a discrete object index at inference. The SRE processes scene and object-centric visual inputs through a transformer to select the optimal obstacle, and the Action Decoder generates rotation-invariant push-grasp parameters for the selected object.

(peripheral accessibility and target proximity) into learned visual representations, providing a strong, sample-efficient starting point that already generalizes well in moderate clutter.

In the second stage, we fine-tune the IL-pretrained weights with proximal policy optimization (PPO) [28], formulating obstacle selection as a discrete Markov Decision Process (MDP). The state s_t is the SRE’s visual input (scene heightmap, target crop, and object crops), and the action $a_t \in \{1, \dots, N\}$ is the index of the selected obstacle. Because the IL stage initiates the policy in a well-structured action space, RL exploration is directed toward the dense, fully occluded regimes where the heuristic degrades. Training runs entirely in simulation with no additional real-robot data.

Each episode samples $N \in [2, 12]$ objects uniformly, with horizon H and discount γ . The per-step reward is

$$r_t = \alpha \cdot \mathbf{1}[\text{success}] \cdot \left(1 + \beta \frac{H-t}{H}\right) + r_{\text{access}}(a_t, s_t) + r_{\text{occl}}(a_t, s_t) \cdot \mathbf{1}[a_t \neq \text{tgt}] + r_{\text{step}}, \quad (2)$$

where r_{access} rewards grasping the target when accessible; the occlusion-shaping term (r_{occl}) rewards obstacle removals by direct target exposure and indirect path clearance; and $r_{\text{step}} < 0$ penalizes unnecessary actions.

Furthermore, we show in our ablation studies (Section VI-F) that removing the encoder leads to a significant drop in task success and planning efficiency, underscoring its critical role in the Unveiler system.

B. Action Decoder

Once the SRE identifies the object that should be removed, the Action Decoder generates the low-level action required to execute the removal. This module is responsible for determining a robust push-grasp action, including position and rotation, tailored to the selected object and the current scene configuration.

The Action Decoder is a fully convolutional network (FCN) that takes two inputs: a depth heightmap of the full scene I_g , and a crop of the selected object O_i extracted from the depth heightmap. These inputs are passed through separate convolutional pathways (see Figure 2). The streams are fused to produce grasp heatmaps across 16 discrete orientations (22.5° increments) for rotation invariance.

The Action Decoder is trained using a supervised cross-entropy loss over grasp maps. During evaluation, we assess performance via metrics such as grasp success rate and number of actions (steps) required to retrieve the target. The expert used to obtain the supervision label is shown in Algorithm 2.

C. Data Collection

Our policy is trained entirely through demonstrations collected in the PyBullet [11] simulation environment. We develop a set of heuristic functions that identify both the optimal obstacle to remove and its corresponding grasp configuration at each decision step (see Algorithms 1 and 2). To ensure data quality, we filter the demonstrations to include only successful manipulation attempts.

To maintain consistency between training and deployment, we enforce strict success criteria for both demonstration collection and policy evaluation. A grasp is considered successful only when it satisfies two key conditions:

- 1) Single-object interaction: The gripper must grasp exactly one object to ensure manipulation stability
- 2) Grasp stability: The grasped object maintains a secure hold when lifted.

These rigorous criteria ensure that our policy learns robust and reliable manipulation strategies that transfer effectively to real-world scenarios. Additionally, using identical success metrics during training and evaluation provides a faithful assessment of the policy’s performance.

Algorithm 1: Obstacle Selection Heuristic

Require: Masks $M = \{M_i\}_{i=1}^N$, target index t

Ensure: Removal order R

- 1: **if** $|M| \leq 3$ **then**
 - 2: **return** $[t]$
 - 3: **end if**
 - 4: Compute $\hat{d}_{\text{edge}}, \hat{d}_{\text{target}}$: normalized boundary and centroid distances
 - 5: $s[i] \leftarrow \hat{d}_{\text{edge}}[i] + \hat{d}_{\text{target}}[i] \quad \forall i \neq t$
 - 6: **return** $R \leftarrow \text{argsort}(s)$
-

Algorithm 2: Grasp Pose Heuristic

Require: Depth heightmap I_g , object mask M_i , workspace bounds $[d_{\min}, d_{\max}]$

Ensure: Push-grasp action $\mathbf{a} = [p_x, p_y, \theta, a_{\text{apt}}]^\top$

- 1: $\mathcal{V} \leftarrow \{(x, y) \mid d_{\min} \leq d(x, y) \leq d_{\max}\}$ {valid grasp pixels within workspace}
 - 2: **if** $\mathcal{V} = \emptyset$ **then**
 - 3: **return** $\mathbf{0}$
 - 4: **end if**
 - 5: $\mathcal{C} \leftarrow \text{contours}(M_i)$ {object boundary pixels}
 - 6: **repeat**
 - 7: $p_1 \sim \mathcal{U}(\mathcal{V})$ {sample grasp center}
 - 8: $\mathcal{P} \leftarrow \{p \in \mathcal{C} \mid \|p - p_1\|_\infty < d_{\text{push}}\}$ {nearby boundary points}
 - 9: **until** $\mathcal{P} \neq \emptyset$
 - 10: $p_2 \sim \mathcal{U}(\mathcal{P})$ {push target on object boundary}
 - 11: $\theta \leftarrow \text{discretize}_{22.5^\circ}(-\arctan 2(p_2 - p_1))$ {quantized push direction}
 - 12: $a_{\text{apt}} \sim \mathcal{U}(\text{aperture limits})$ {gripper opening width}
 - 13: **return** $\mathbf{a} = [1.05 \cdot p_1, \theta, a_{\text{apt}}]^\top$
-

V. PROPERTIES OF THE DECOMPOSED POLICY

The factorization equation (Eqn. 1) defined in Section III is not merely an architectural convenience. It induces two properties with direct implications for how the system learns and how failures can be diagnosed.

1) *Object-centric inductive bias:* The SRE architecture encodes structure that a monolithic policy must discover implicitly. The target is always the cross-attention query, anchoring learned representations to target-relative spatial context from the first gradient update. Per-object crops make the model equivariant to instance ordering, so the same selection behavior generalizes across object counts and configurations not seen during training.

2) *Additive error decomposition:* Because selection and execution are separate, their failure modes are also separate. If the SRE selects a suboptimal object on a fraction ϵ_{SRE} of steps and each wrong choice costs at most Δ in expected progress, the total performance gap of the actual SRE policy ($J(\pi)$) to an ideal policy ($J(\pi^*)$) is bounded by

$$J(\pi^*) - J(\pi) \leq H \cdot \Delta \cdot \epsilon_{\text{SRE}} + \epsilon_{\text{exec}} \quad (3)$$

where $H \leq N$ is the episode horizon (one step per removal), Δ is the worst-case cost of a single wrong object pick, ϵ_{SRE} is the SRE’s object misclassification rate (measured as held-out top-1 error), and ϵ_{exec} is the Action Decoder’s execution error given the correct object. Such linear horizon dependence on per-step classification error is standard in imitation-learning reduction analyses [29], [30]. The two terms are additive, not multiplicative, which means neither source compounds the other.

VI. EXPERIMENTS

We evaluate our system in both simulated and real-world settings to assess its effectiveness in retrieving occluded target objects from cluttered scenes. The evaluation aims to answer the following questions: (i) How effectively can Unveiler retrieve targets across varying clutter levels? (ii) How does Unveiler compare to strong baselines? (iii) How well does it generalize to unseen conditions? (iv) What is the impact of each architectural component?

A. Baselines

We evaluate Unveiler against the following state-of-the-art baselines for object retrieval and manipulation in cluttered scenes: **Target-Conditioned PPG** [3], **Heur** (the heuristic policies used to train Unveiler), **ACT** [31], **CLIP-Grounding** [9], **GPT-4o** [5], **VILG** [8], and **ThinkGrasp** [10].

B. Evaluation Metrics

We evaluate our system using two complementary metrics that capture planning quality and execution robustness:

- **Task Completion Rate (%)**: The percentage of test episodes in which the robot successfully retrieves the target object.
- **Action Efficiency (Steps)**: The average number of actions taken, including obstacle removals and the final grasp.

Together, these metrics provide a holistic view of system performance, spanning both high-level spatial reasoning (via encoder predictions) and low-level manipulation robustness (via decoder execution).

C. Computational Efficiency Analysis

Unveiler achieves strong computational efficiency as shown in Table I. These results highlight how Unveiler maintains near real-time efficiency by separating spatial reasoning from action generation, avoiding end-to-end overhead and enabling deployment on resource-constrained robotic systems.

D. Simulation Experiments

We validated the robustness of our system through testing on objects of varying scales from both YCB [32] and KIT [33] datasets, showing consistent performance across different object size distributions. We categorized the objects into two sets (seen and unseen sets) and used one for training (seen) and the other for evaluation (unseen). Each condition in Table II is evaluated over 30 episodes per method.

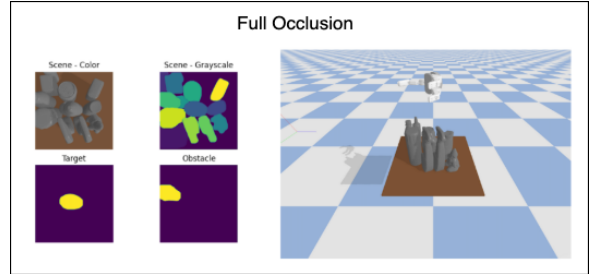
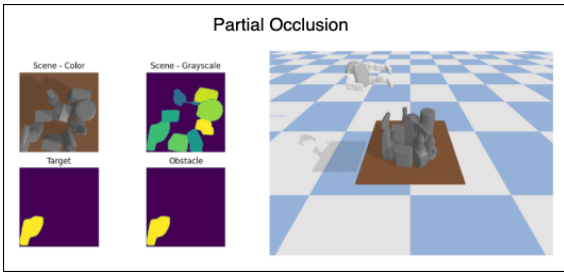


Fig. 3. Example scenes illustrating occlusion levels of the target object. (Left) The target object is partially occluded, with some visible surface area. (Right) The target object is fully occluded, entirely covered by surrounding objects, and not directly visible in the input view.

TABLE I
COMPUTATIONAL EFFICIENCY COMPARISON

Method	Params. (M)	Est. Inference (ms)	Efficiency (\uparrow)
Unveiler (Ours)	83.03	~ 260	1.0x
VILG	156.26	$\sim 29,300^a$	0.093–0.0047x
GPT-4o*	-	$> 6000^b$	$< 0.043x$
ThinkGrasp ⁺	-	$> 6000^b$	$< 0.043x$

*,+ Parameter count unavailable; requires cloud API inference.

^a Average shown; actual range 2807–55,741.9 ms.

^b Dependent on API latency; range is above 6000 ms.

Our evaluation (as seen in Table II) demonstrates that Unveiler maintains superior performance across varying scene complexity while exhibiting more efficient planning compared to baseline approaches. We selected VILG [8] and ThinkGrasp [10] as baselines in addition to other approaches because they represent some of the most recent vision-based approaches for grasping in cluttered environments. VILG jointly integrates vision, language, and action without handcrafted grounding rules, making it highly relevant to our focus on relational reasoning. ThinkGrasp leverages GPT-4o for obstacle selection and part-level grasping to directly address sequential object removal, which aligns closely with the core challenge tackled by Unveiler. The results reveal three critical insights: first, Unveiler consistently requires fewer planning steps across all conditions, averaging 1.17–3.71 steps compared to baselines that often exceed 4+ steps in complex scenarios. This efficiency advantage is particularly pronounced in cluttered environments where methods like PPG and VILG require significantly more steps due to suboptimal sequencing decisions. Second, while all methods experience performance drops with increased clutter and occlusion, Unveiler demonstrates superior robustness, maintaining 53.8% success rate in the most challenging scenarios (9–12 objects with full occlusion) while most baselines drop below 35%, with some failing entirely (ACT and PPG show no completions). Third, the results expose method-specific limitations: GPT-4o exhibits planning inefficiency due to misalignment between its predictions and optimal removal sequences, requiring up to 4.22 steps in dense scenes, while the heuristic baseline fails dramatically as scene complexity increases, despite reasonable completion rates in low-clutter conditions. These results validate Unveiler’s core contribution: effective reasoning about obstacle removal sequences that translates to both higher task completion rates and

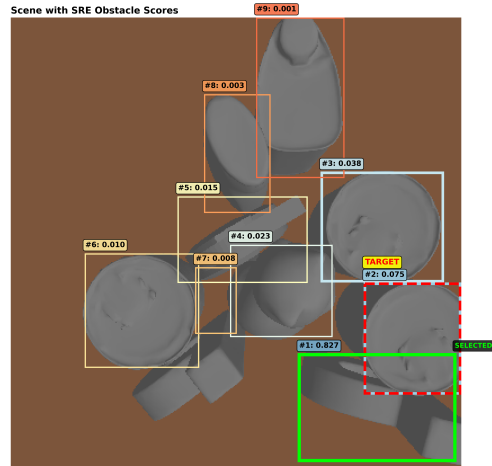


Fig. 4. Scene overlay with selection probabilities. Target outlined in red, selected obstacle in green.

more efficient planning across the full spectrum of scene complexity.

E. Spatial Reasoning and Interpretability Analysis

The selection probability visualization in Figure 4 demonstrates that the SRE learns to identify optimal obstacles based on spatial relationships rather than simple proximity. The model consistently avoids selecting objects that are difficult to grasp due to workspace boundaries or neighboring objects, and shows sensitivity to cascading effects where removal might destabilize the scene. The interpretable selection probabilities provide transparency into the decision-making process, which is crucial for applications where understanding the robot’s reasoning is essential.

F. Ablation Studies

To understand the contribution of the individual components of Unveiler, we conducted a series of ablation studies, and the results are shown in Table III.

- **SRE w/o RL finetuning:** Using only SRE without RL finetuning, the system underperforms relative to the full Unveiler system by **3.3%**, confirming that RL discovers strategies that the heuristic supervisor cannot provide.
- **No SRE:** Removing the spatial relationship encoder reduces completion by **13.6%** under full occlusion while slightly improving partial occlusion performance

TABLE II

PERFORMANCE COMPARISON OF GPT-4o, CLIP-GROUNDING, VILG, THINKGRASP, ACT, PPG, HEUR, AND UNVEILER (OURS) ACROSS DIFFERENT CLUTTER DENSITIES AND OCCLUSION LEVELS. METRICS: TASK COMPLETION (%) AND AVERAGE PLANNING STEPS.

Clut.	Occl.	GPT-4o		CLIP-Ground.		VILG		ThinkGrasp		ACT		PPG		Heur		Unveiler (Ours)	
		%	Steps	%	Steps	%	Steps	%	Steps	%	Steps	%	Steps	%	Steps	%	Steps
2-6	Partial	86.0	1.50	80.5	1.67	75.0	3.0	73.3	3.00	45.2	1.14	40.6	4.42	87.3	2.35	96.1	1.32
2-6	Full	66.7	2.50	60.3	2.11	50.0	2.86	53.3	2.25	40.0	1.00	50.3	4.27	67.5	2.30	89.3	1.87
6-9	Partial	80.0	1.81	67.2	3.10	80.0	3.17	66.7	3.29	40.0	1.00	7.5	6.00	67.5	2.55	97.6	1.43
6-9	Full	60.0	4.22	66.7	4.20	40.0	3.33	60.0	3.78	10.0	1.00	4.4	3.00	47.8	3.43	90.0	3.31
9-12	Partial	66.7	3.10	53.0	4.38	46.7	2.86	46.7	3.42	25.7	1.00	4.4	4.00	50.0	3.40	92.6	2.86
9-12	Full	26.7	3.00	20.0	4.67	33.3	3.4	33.3	3.56	-	-	-	-	20.0	3.17	53.8	3.71

TABLE III

ABLATION STUDY. ARCHITECTURAL VARIANTS EVALUATED AT 6-9 OBJECT DENSITY; DENSITY GENERALIZATION SHOWN FOR NO SRE VS. FULL UNVEILER. METRICS: TASK COMPLETION (%) AND AVERAGE PLANNING STEPS.

Method	Density	Partial		Full	
		%	Steps	%	Steps
No SRE	6-9	96.0	2.10	76.0	3.39
Multi-Obstacle SRE	6-9	73.3	3.44	60.0	4.90
Binary Mask Input	6-9	56.7	2.94	36.7	4.55
Unveiler (Ours)	6-9	97.6	1.43	90.0	3.31
No SRE	9-12	84.0	2.91	46.0	6.39
SRE w/o RL finetuning	9-12	88.4	2.64	52.0	4.11
Unveiler (Ours)	9-12	92.6	2.86	53.8	3.71

by **3.4%**, demonstrating its critical role in complex scenarios.

- **Multi-Obstacle Selection:** Predicting all removable obstacles in one shot degrades performance by **25.2%** (partial) and **33.3%** (full occlusion), demonstrating the importance of sequential reasoning.
- **Binary Mask Input:** Replacing rich object crops with binary masks causes significant drops of **42.1%** (partial) and **53.3%** (full occlusion), validating the importance of detailed visual representations.

These studies confirm that each architectural component contributes meaningfully to overall performance, with their removal leading to measurable performance degradation.

G. Demonstration on a Real Robot

We validate our system on a Dofbot-Pro manipulator (as shown in Figure 1) equipped with a parallel gripper. The perception system consists of a calibrated Intel RealSense camera mounted at the top of the robot base, providing top-down RGB-D data at 480×640 resolution.

The properties of the architecture facilitate zero-shot transfer. First, both components operate on depth heightmaps rather than RGB, eliminating color and texture domain shift. Second, the top-down camera geometry used in deployment matches the simulator, preserving spatial scale and centroid

coordinates. Third, the Action Decoder’s rotation-invariant prediction aggregates over 16 orientations, making grasps robust to small pose deviations between the simulated and physical object placements. The heightmap was generated directly from the single top-down Intel RealSense camera mounted on the robot base. While this provides a less complete 3D point cloud than the dual-camera setup used in simulation (which mitigates self-occlusion from the robot’s arm), our policy outperformed other approaches in real-world trials as shown in Table IV. The only real-world adaptation was a one-time geometric recalibration of the workspace bounds to the physical table extent; no learned component was retrained or fine-tuned. Critically, arm kinematics are encoded solely in these non-learned bounds and not in the policy itself, so the shift from the Barrett hand to the Dofbot-Pro introduces no domain gap for the SRE. This confirms that the domain gap between simulated and physical heightmaps does not significantly degrade performance.

H. Scene Reasoning Evaluation on Real Images

TABLE IV
OBJECT SELECTION ACCURACY ON REAL SCENES ($N = 35$)

Method	2 - 4 (%)	5 - 8 (%)
CLIP-Grounding	65	37
GPT-4o	40	26
SRE (Ours)	60	54

To isolate the SRE’s spatial reasoning from execution noise, we evaluate object-selection accuracy directly on 35 real top-down tabletop scenes. This decoupled evaluation is natural given the factored architecture: the SRE’s discrete output can be assessed independently of any physical arm.

Results are shown in Table IV. In sparse scenes (2-4 objects), CLIP-Grounding performs comparably, as appearance similarity suffices when occlusion is limited. In denser scenes (5-8 objects), the SRE (54%) substantially outperforms CLIP-Grounding (37%) and GPT-4o (26%), confirming that geometric reasoning about occlusion and periphery, not appearance similarity, drives the SRE’s advantage in clutter. These results confirm that the learned spatial reasoning transfers to real scenes without any fine-tuning.

VII. CONCLUSION

We have presented Unveiler, a decoupled framework that separates spatial reasoning from action execution for long-horizon object manipulation in cluttered environments. Unlike proximity-based approaches, our method identifies optimal removal sequences by reasoning about object dimensions, grasp accessibility, workspace boundaries, and cascading stability effects, enabling more robust manipulation planning in complex scenarios.

Our key insights are fourfold: the SRE’s sequential decision-making effectively models complex object dependencies for long-horizon spatial reasoning; our lightweight architecture (83.03M parameters) achieves state-of-the-art performance with near real-time inference (~ 260 ms); the interpretable obstacle selection process provides crucial transparency. RL fine-tuning improves over the IL-only baseline in the hardest conditions, confirming the policy is not bounded by its training heuristic.

Unveiler’s spatial reasoning could complement VLA models by serving as a specialized data generator for cluttered manipulation scenarios or as a modular spatial reasoning component that enhances VLA performance on complex sequential tasks. The demonstrated effectiveness of specialized, object-centric reasoning suggests continued relevance for purpose-built architectures, providing a pathway for deploying sophisticated manipulation capabilities on resource-constrained robotic systems.

REFERENCES

- [1] B. Tang, M. Corsaro, G. Konidaris, S. Nikolaidis, and S. Tellex, “Learning collaborative pushing and grasping policies in dense clutter,” in *2021 IEEE International Conference on Robotics and Automation (ICRA)*. IEEE, 2021, pp. 6177–6184.
- [2] A. Zeng, P. Florence, J. Tompson, S. Welker, J. Chien, M. Attarian, T. Armstrong, I. Krasin, D. Duong, V. Sindhwani *et al.*, “Transporter networks: Rearranging the visual world for robotic manipulation,” in *Conference on Robot Learning*. PMLR, 2021, pp. 726–747.
- [3] M. Kiatos, I. Sarantopoulos, L. Koutras, S. Malassiotis, and Z. Doulgeri, “Learning push-grasping in dense clutter,” *IEEE Robotics and Automation Letters*, vol. 7, no. 4, pp. 8783–8790, 2022.
- [4] D. Li, C. Zhao, S. Yang, R. Song, X. Li, and W. Zhang, “Mpgnet: Learning move-push-grasping synergy for target-oriented grasping in occluded scenes,” in *2024 IEEE/RSJ International Conference on Intelligent Robots and Systems (IROS)*. IEEE, 2024, pp. 5064–5071.
- [5] A. Hurst, A. Lerer, A. P. Goucher, A. Perelman, A. Ramesh, A. Clark, A. Ostrow, A. Welihinda, A. Hayes, A. Radford *et al.*, “Gpt-4o system card,” *arXiv preprint arXiv:2410.21276*, 2024.
- [6] K. Black, N. Brown, D. Driess, A. Esmail, M. Equi, C. Finn, N. Fusai, L. Groom, K. Hausman, B. Ichter *et al.*, “pi0: A vision-language-action flow model for general robot control,” *arXiv preprint arXiv:2410.24164*, 2024.
- [7] J. Bjorck, F. Castañeda, N. Cherniadev, X. Da, R. Ding, L. Fan, Y. Fang, D. Fox, F. Hu, S. Huang *et al.*, “Gr00t n1: An open foundation model for generalist humanoid robots,” *arXiv preprint arXiv:2503.14734*, 2025.
- [8] K. Xu, S. Zhao, Z. Zhou, Z. Li, H. Pi, Y. Zhu, Y. Wang, and R. Xiong, “A joint modeling of vision-language-action for target-oriented grasping in clutter,” pp. 11 597–11 604, 2023.
- [9] A. Radford, J. W. Kim, C. Hallacy, A. Ramesh, G. Goh, S. Agarwal, G. Sastry, A. Askell, P. Mishkin, J. Clark *et al.*, “Learning transferable visual models from natural language supervision,” in *International conference on machine learning*. PMLR, 2021, pp. 8748–8763.
- [10] Y. Qian, X. Zhu, O. Biza, S. Jiang, L. Zhao, H. Huang, Y. Qi, and R. Platt, “Thinkgrasp: A vision-language system for strategic part grasping in clutter,” *arXiv preprint arXiv:2407.11298*, 2024.
- [11] E. Coumans and Y. Bai, “Pybullet, a python module for physics simulation for games, robotics and machine learning,” <http://pybullet.org>, 2016–2021.
- [12] A. Zeng, S. Song, S. Welker, J. Lee, A. Rodriguez, and T. Funkhouser, “Learning synergies between pushing and grasping with self-supervised deep reinforcement learning,” in *2018 IEEE/RSJ International Conference on Intelligent Robots and Systems (IROS)*. IEEE, 2018, pp. 4238–4245.
- [13] Y. Deng, X. Guo, Y. Wei, K. Lu, B. Fang, D. Guo, H. Liu, and F. Sun, “Deep reinforcement learning for robotic pushing and picking in cluttered environment,” in *2019 IEEE/RSJ International Conference on Intelligent Robots and Systems (IROS)*. IEEE, 2019, pp. 619–626.
- [14] Y. Yang, H. Liang, and C. Choi, “A deep learning approach to grasping the invisible,” *IEEE Robotics and Automation Letters*, vol. 5, no. 2, pp. 2232–2239, 2020.
- [15] Y. Jiang, A. Gupta, Z. Zhang, G. Wang, Y. Dou, Y. Chen, L. Fei-Fei, A. Anandkumar, Y. Zhu, and L. Fan, “Vima: General robot manipulation with multimodal prompts,” *arXiv preprint arXiv:2210.03094*, vol. 2, no. 3, p. 6, 2022.
- [16] Y. Zhu, A. Joshi, P. Stone, and Y. Zhu, “Viola: Imitation learning for vision-based manipulation with object proposal priors,” in *Conference on Robot Learning*. PMLR, 2023, pp. 1199–1210.
- [17] Y. Zhu, Z. Jiang, P. Stone, and Y. Zhu, “Learning generalizable manipulation policies with object-centric 3d representations,” *arXiv preprint arXiv:2310.14386*, 2023.
- [18] S. Ferraro, P. Mazzaglia, T. Verbelen, and B. Dhoedt, “Focus: object-centric world models for robotic manipulation,” *Frontiers in Neuro-robotics*, vol. 19, p. 1585386, 2025.
- [19] C. Eze and C. Crick, “Learning by watching: A review of video-based learning approaches for robot manipulation,” *IEEE Access*, 2025.
- [20] L. Meng, Z. Qi, L. Shuchang, W. Chunlei, M. Yujing, C. Guangliang, and Y. Chenguang, “Ovgnet: A unified visual-linguistic framework for open-vocabulary robotic grasping,” *arXiv preprint arXiv:2407.13175*, 2024.
- [21] X. Lou, Y. Yang, and C. Choi, “Learning object relations with graph neural networks for target-driven grasping in dense clutter,” in *2022 International Conference on Robotics and Automation (ICRA)*. IEEE, 2022, pp. 742–748.
- [22] E. Li, H. Feng, S. Zhang, and Y. Fu, “Learning target-oriented push-grasping synergy in clutter with action space decoupling,” *IEEE Robotics and Automation Letters*, vol. 7, no. 4, pp. 11 966–11 973, 2022.
- [23] Y. Wang, K. Mokhtar, C. Heemskerk, and H. Kasaei, “Self-supervised learning for joint pushing and grasping policies in highly cluttered environments,” in *2024 IEEE International Conference on Robotics and Automation (ICRA)*. IEEE, 2024, pp. 13 840–13 847.
- [24] K. Xu, H. Yu, Q. Lai, Y. Wang, and R. Xiong, “Efficient learning of goal-oriented push-grasping synergy in clutter,” *IEEE Robotics and Automation Letters*, vol. 6, no. 4, pp. 6337–6344, 2021.
- [25] A. Vaswani, “Attention is all you need,” *Advances in Neural Information Processing Systems*, 2017.
- [26] K. He, X. Zhang, S. Ren, and J. Sun, “Deep residual learning for image recognition,” in *Proceedings of the IEEE conference on computer vision and pattern recognition*, 2016, pp. 770–778.
- [27] O. Russakovsky, J. Deng, H. Su, J. Krause, S. Satheesh, S. Ma, Z. Huang, A. Karpathy, A. Khosla, M. Bernstein *et al.*, “Imagenet large scale visual recognition challenge,” *International journal of computer vision*, vol. 115, pp. 211–252, 2015.
- [28] J. Schulman, F. Wolski, P. Dhariwal, A. Radford, and O. Klimov, “Proximal policy optimization algorithms,” *arXiv preprint arXiv:1707.06347*, 2017.
- [29] S. Ross and J. A. Bagnell, “Efficient reductions for imitation learning,” in *Proceedings of the Thirteenth International Conference on Artificial Intelligence and Statistics (AISTATS)*, 2010.
- [30] S. Ross, G. Gordon, and J. A. Bagnell, “A reduction of imitation learning and structured prediction to no-regret online learning,” in *Proceedings of the Fourteenth International Conference on Artificial Intelligence and Statistics (AISTATS)*, 2011.
- [31] T. Z. Zhao, V. Kumar, S. Levine, and C. Finn, “Learning fine-grained bimanual manipulation with low-cost hardware,” *arXiv preprint arXiv:2304.13705*, 2023.
- [32] B. Calli, A. Singh, A. Walsman, S. Srinivasa, P. Abbeel, and A. M. Dollar, “The ycb object and model set: Towards common benchmarks for manipulation research,” in *2015 international conference on advanced robotics (ICAR)*. IEEE, 2015, pp. 510–517.

- [33] A. Kasper, Z. Xue, and R. Dillmann, "The kit object models database: An object model database for object recognition, localization and manipulation in service robotics," *The International Journal of Robotics Research*, vol. 31, no. 8, pp. 927–934, 2012.